Firing Rate-dependent Phase Responses of Purkinje Cells Support Transient Oscillations

Yunliang Zang & Erik De Schutter
Computational Neuroscience Unit, Okinawa Institute of Science and Technology Graduate University, Okinawa 904-0495, Japan

Abstract

Both spike rate and timing transmit information in the brain, yet how rate-modulated cellular properties affect spike timing is largely unexplored. Phase response curves (PRCs), quantifying how a neuron transforms input to output by spike timing, exhibit strong rate-adaptation, but its mechanism and relevance for network output are poorly understood. Using our Purkinje cell (PC) model and pyramidal neuron model, we demonstrate that the rate-adaptation is caused by rate-dependent subthreshold membrane potentials efficiently regulating the activation of Na^+ channels. Then we use a realistic PC network model to examine how rate-dependent responses synchronize spikes in the scenario of reciprocal inhibition-caused high-frequency oscillations. Large and broad PRCs at high rates increase oscillation power and spike correlations. The irregularity of spiking and the network connectivity also regulate oscillations. The combination of these factors enables transient oscillations between fast-spiking neurons. Our work demonstrates that rate-adaptation of PRCs can spatio-temporally organize neuronal output.

Introduction

The propensity of neurons to fire synchronously depends on the interaction between cellular and network properties (Ermentrout et al., 2001). A phase response curve (PRC) quantifies how a weak stimulus exerted at different phases during the interspike interval can shift subsequent spike timing in repetitively firing neurons (Ermentrout et al., 2001; Gutkin et al., 2005). Essentially, the PRC measures how a neuron transforms an input to output by spike timing. Therefore, it determines the potential of network synchronization (Ermentrout et al., 2001; Ermentrout et al., 2008; Gutkin et al., 2005; Smeal et al., 2010). The PRC is not static and shows significant adaptation with spike rate. It was theoretically predicted that PRCs decrease at high firing rates in pyramidal neurons (Gutkin et al., 2005), which unfortunately did not match later experimental observations showing an increased PRC peak at higher rates (Tsubo et al., 2007). Similarly, for PRCs in Purkinje Cells (PCs), the responses to weak stimuli at low spiking rates are small and surprisingly flat. With increased rates, responses in later phases become phase-dependent, with onset-phases left-shifted and gradually increasing peak amplitudes, which has never been theoretically replicated or explained (Couto et al., 2015; Phoka et al., 2010), nor has its effect in synchronizing spike outputs been explored.

On the circuit level, reciprocal inhibition causing high frequency oscillations has been observed in many regions of the brain such as cerebellum and hippocampus (Bartos et al., 2002; Cheron et al., 2004; de Solages et al., 2008) . However, how cellular properties such as PRCs regulate the oscillations is still poorly understood. Furthermore, the functional importance of oscillations in information transmission will be largely determined by their spatio-temporal scale, which is difficult to predict given the hard-wired inhibitory connections. Since the PRC is spike rate-dependent, it is interesting to explore whether this cellular property can dynamically regulate the spatial range of oscillations based on spike rate changes.

To examine the mechanism of rate-dependent PRCs, we use our physiologically detailed PC model (Zang et al., 2018) and a simple pyramidal neuron model to explore the rate adaptation of PRCs. By analyzing simulation data and *in vitro* experimental data (Rancz and Hausser, 2010), we identify that rate-dependent subthreshold membrane potentials can modulate the activation of Na^+ channels to shape neuronal PRC profiles. We also build a PC network model connected by inhibitory axon collaterals to simulate high-frequency oscillations (de Solages et al., 2008; Witter et al., 2016). Rate adaptation of PRCs can increase the power of oscillations to link the rate with spike timing. Moreover, firing irregularity and network connectivity also regulate the oscillation level. The combination of these factors enables PC spikes uncorrelated at low basal rates to become transiently correlated in a subgroup of cells at high rates.

Results

PRC Exhibits Rate Adaptation in PCs

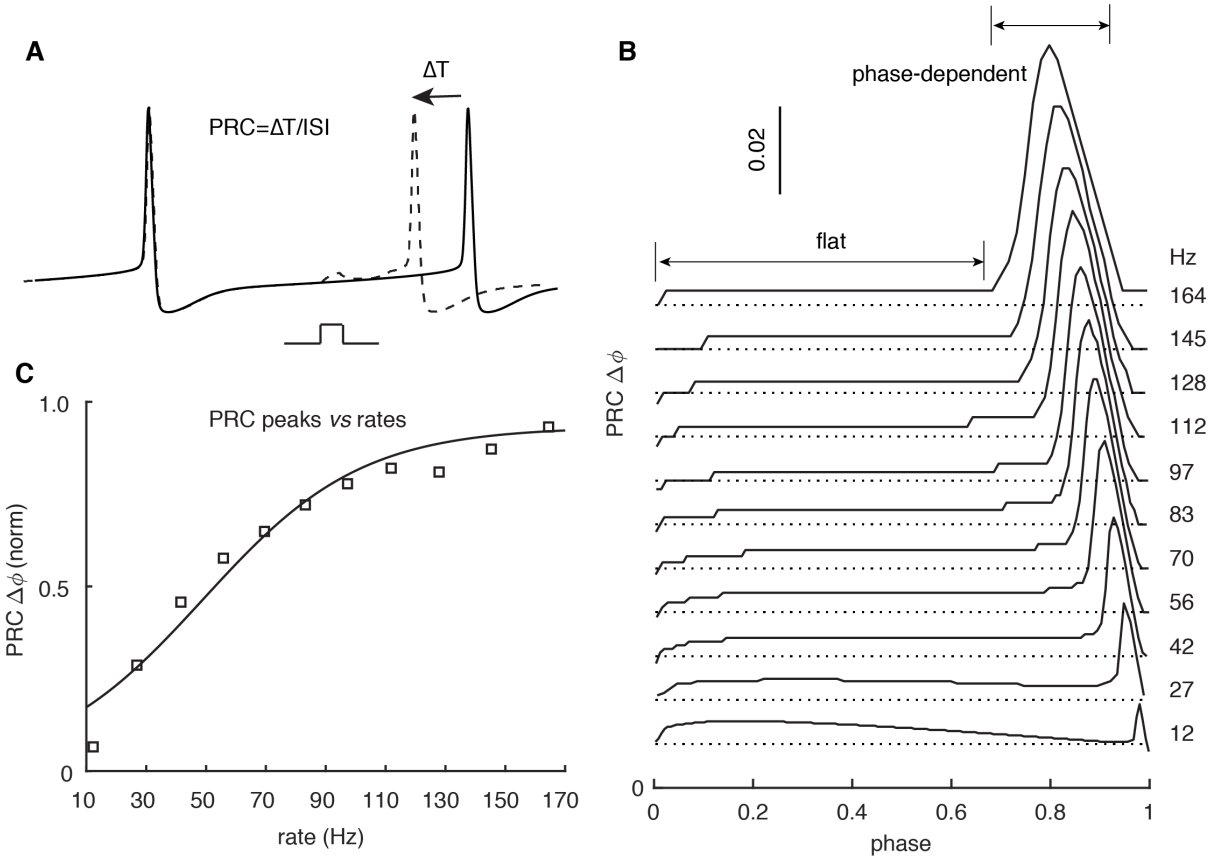

Figure 1. PRC Exhibits Strong Rate Adaptation in PC model
(**A**) Schematic representation of the definition and computation of PRCs. The current pulse has a duration of 0.5 ms and an amplitude of 50 pA. Different spike rates were achieved by somatic current injection (Couto et al., 2015; Phoka et al., 2010). (**B**) The rate adaptation of flat and phase-dependent parts of PRCs. (**C**) PRC peaks at different rates fitted by the Boltzmann function.

PRCs were obtained by repeatedly exerting a weak stimulus at different phases of the interspike interval (ISI). The resulting change in ISI relative to original ISI corresponds to the PRC value at that phase (Fig. 1A). All previous abstract and detailed PC models failed to replicate the experimentally observed rate-adaptation of PRCs (Akemann and Knopfel, 2006; Couto et al., 2015; De Schutter and Bower, 1994; Khaliq et al., 2003; Phoka et al., 2010). Our recent PC model was well constrained against a wide range of experimental data (Zang et al.,

2018). Here, we explored whether this model can capture the rate-adaptation of PRCs under similar conditions. When the PC model fires at 12 Hz, responses (phase advances) to weak stimuli are small and nearly flat for the whole ISI (Fig. 1B). Only at a very narrow late phase do the responses become phase-dependent, increasing slightly. With increased rates, the responses remain small and flat during early phases. However, later, phase-dependent responses gradually become larger, with onset-phases shifted left. In agreement with experiments under the same stimulus conditions (Phoka et al., 2010), the peak of PRCs finally became saturated at ~ 0.06 at high rates. The relationship between normalized PRC peaks and rates can be fitted by the Boltzman function and matches experimental data (Fig. 1C, fitted with $1/(1 + e^{-(rate-a)/b})$, a = 49.1, b = 26.4 in the model *vs* a = 44.1 and b = 20.5 in experiments (Couto et al., 2015). PRCs in our model show similar rate adaption with inhibitory stimuli (phase delay, Fig. S1A). Rate-adaptive PRCs require the presence of a dendrite in the PC model (not shown), but the dendrite can be passive (Fig. S1B). We also tested the effect of increasing stimulus amplitude on PRC adaptation. Increasing stimulus amplitude consistently shifted onset-phases of phase-dependent parts to the left and increased their amplitudes (Fig. S1C).

To unveil the biophysical principles governing rate-adaptive PRC profiles, we need to answer three questions: Why are responses flat in early phases? Why do responses become phase-dependent during later phases? What changes cause the rate adaptation of PRCs?

The Biophysical Mechanism of Rate Adaptation of PRCs in PCs

To answer the aforementioned questions, we examine how spike properties vary with rate and find that the facilitation of Na^+ currents relative to K^+ currents, due to elevated subthreshold membrane potentials at high rates, underlies the rate adaptation of PRCs. After each spike, there is a pronounced after-hyperpolarization (AHP) caused by the large conductance Ca^{2+}-activated K^+ current, and subsequently the membrane potential gradually depolarizes due to intrinsic Na^+ currents and dendritic axial current (Zang et al., 2018). As confirmed by re-analyzing *in vitro* somatic membrane potential recordings (shared by Ede Rancz and Michael Häusser (Rancz and Hausser, 2010)), subthreshold membrane potential levels are significantly elevated at high rates, but spike thresholds rise only slightly with rate (Fig. 2A). This means the ISI phase where Na^+ activation threshold (~ - 55 mV for 0.5% activation in PCs (Khaliq et al., 2003; Zang et al., 2018)) is crossed shifts left and larger phase ranges of membrane potentials are above the threshold at high rates (Fig. 2B).

During early phases of all rates, membrane potentials are distant from the Na^+ activation threshold (Fig. 2A,B). The depolarizations to weak stimuli fail to activate sufficient Na^+ channels to speed up voltage trajectories, and phase advances are caused by just the passive depolarizations (Fig. 2C). Consequently, phase advances in early phases are small and flat (or phase independent). At later phases, membrane potentials gradually approach and surpass the Na^+ activation threshold. Stimulus-evoked depolarizations activate more Na^+ channels to speed up trajectories in return. Therefore, phase advances become large and phase- (actually voltage-) dependent. At low rates, membrane potentials are below the Na^+ activation threshold during nearly the entire interspike period (Fig. 2B). Responses are thus generally phase-independent. At high rates, onset-phases of phase-dependent responses parallel the left shifts of Na^+ activation threshold-corresponding phases, due to elevated subthreshold membrane potentials. Because high rate-corresponding elevated membrane potentials have larger slopes at the foot of the Na^+ activation curve, a same ΔV (passive depolarization) activates more Na^+ channels and consequently causes larger PRC peaks at high rates (Fig. 2C,D). Under all conditions (except phase = 0.2, 162 Hz), stimulus-evoked depolarizations also increase outward currents, but this increase is smaller than that of inward currents (mainly Na^+) due to the high activation threshold of K^+ currents (mainly Kv3) in PCs (Martina et al., 2003; Zang et al., 2018). As the

stimulus becomes stronger, its triggered passive depolarization increases and the required pre-stimulus membrane potential (phase) to reach Na^+ activation threshold is lowered (left shifted). Thus, increasing the stimulus amplitude not only increases the PRC peaks, but also shifts the onset-phases of phase-dependent responses to the left (Fig. S1C).

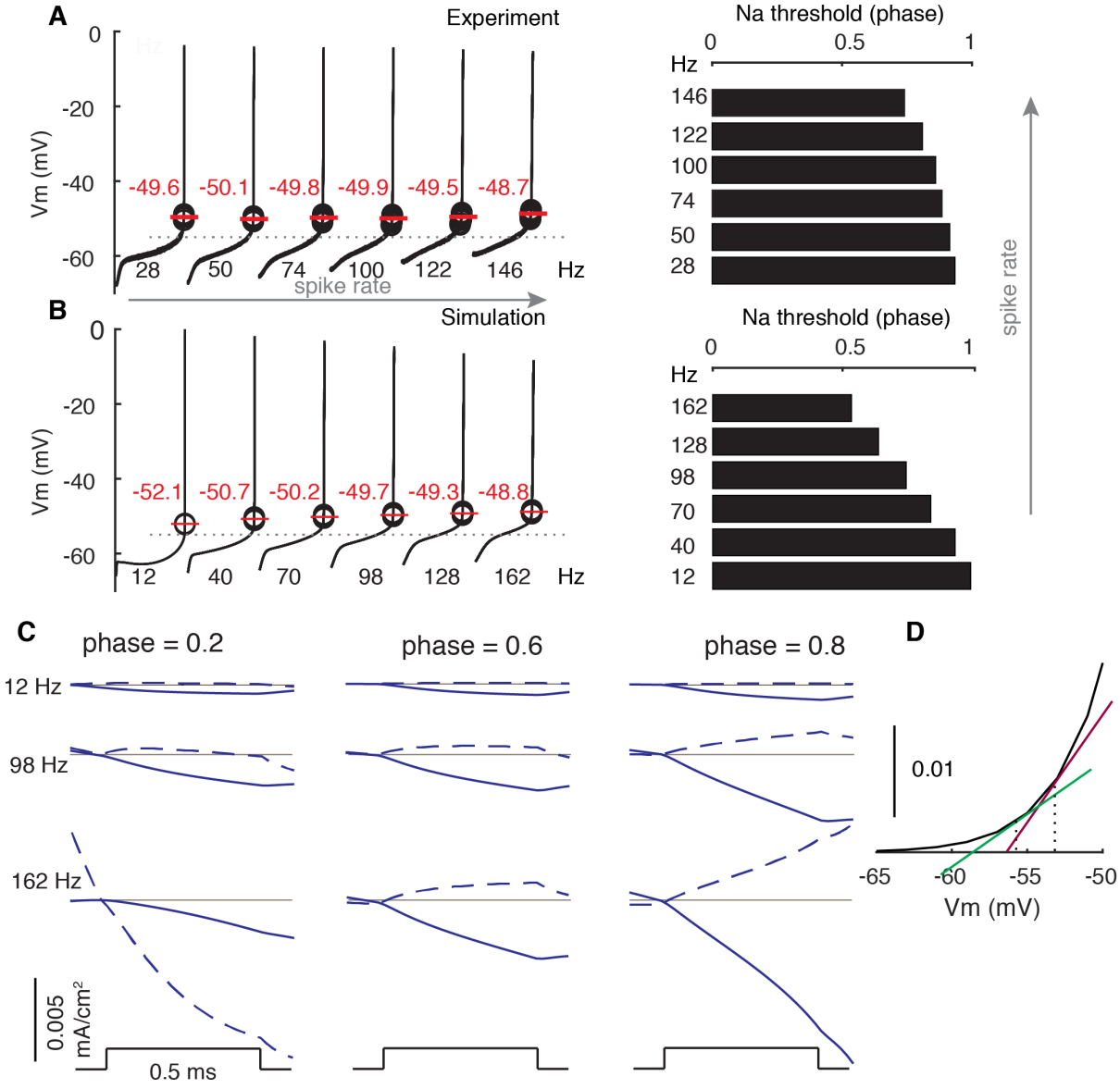

Figure 2. Modulated Subthreshold Membrane Potentials Account for the Rate-adaptation of PRCs.

(**A** and **B**) Experimental and simulated voltage trajectories in PCs during ISIs at different rates. The model used (Zang et al., 2018) was not fitted to this specific experimental data. Spike thresholds at different rates are labeled in plots. The Na^+ activation threshold is defined as -55 mV (stippled line). Right plots show left-shifted Na^+-activation threshold-corresponding phases at high rates. (**C**) Stimulus-triggered variations of inward ionic currents (solid) and outward ionic currents (dashed) at different phases and rates. Ionic currents are shifted to 0 (grey line) at the time of stimulus to compare their relative changes. At phase = 0.2, the outward current is still decreasing due to the inactivation of the large conductance Ca^{2+}-activated K^+ current at 162 Hz. (**D**) Larger slopes of the Na^+ activation curve at high membrane potentials.

General Effect of Subthreshold Membrane Potentials on Shaping PRCs

Here, we examine whether the critical role of subthreshold membrane potentials in shaping PRC profiles also applies to other neuron types. A frequently used pyramidal neuron model, the Traub model (Ermentrout et al., 2001) was tested. It shows an opposite rate-adaptation of PRCs compared to PCs (Fig. 3A). In the Traub model, responses become smaller and relatively phase-independent at high rates. In contrast to PCs, subthreshold membrane potentials are significantly lower at high rates due to the accumulation of delayed rectifier K^+ current (kdr, Fig. 3B,C), which has a low activation threshold and large conductance. The lower subthreshold membrane potentials are far below the Na^+-activation threshold, making responses to weak stimuli passive at high rates. Accordingly, PRCs in the model become smaller and relatively phase-independent at high rates, this was not confirmed in more recent experimental recordings(Tsubo et al., 2007). We minimally modified the Traub model by reducing the conductance of the kdr current, raising its activation threshold and increasing the AHP current (details in **Methods**) (Fig. 3D-F). With these modifications, subthreshold membrane potentials are significantly elevated at high spiking rates. Accordingly, onset-phases of phase-dependent responses shift left and peaks increase at high rates. These simulation results confirm that, for any type of neuron, spike rate-dependent subthreshold membrane potentials and their effect on nonlinear activation of Na^+ currents are crucial in shaping neuronal PRC profiles.

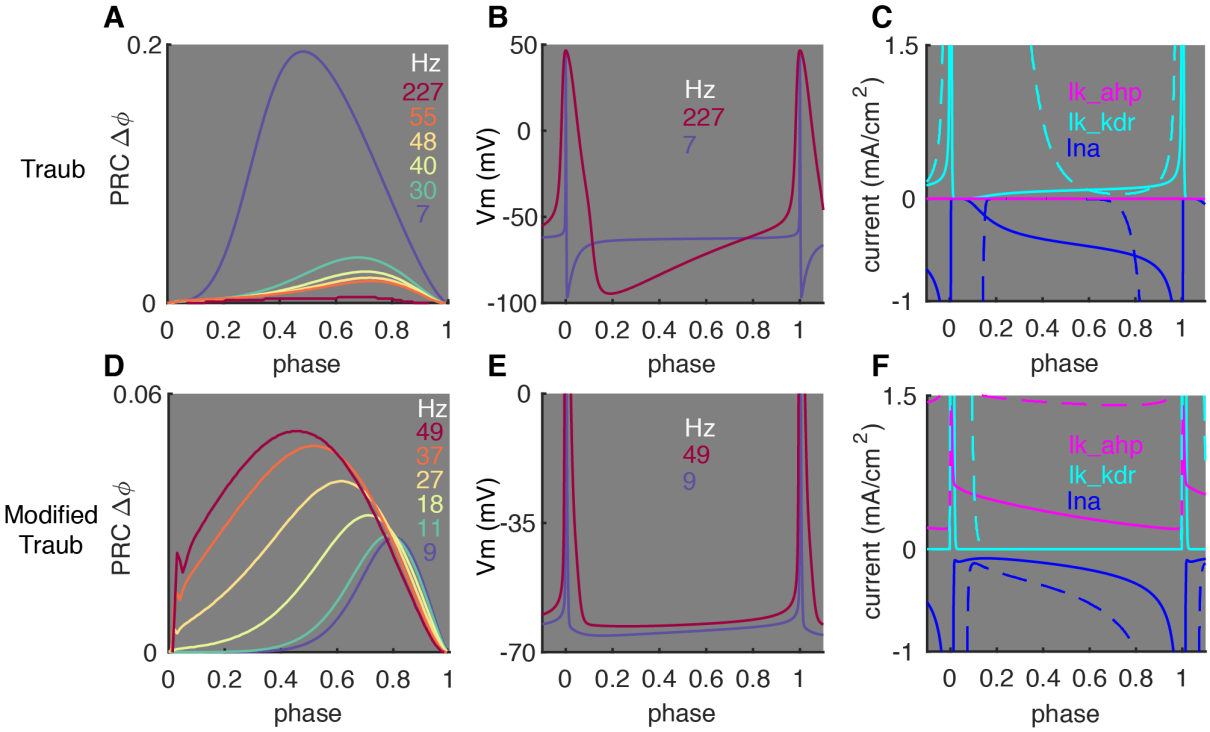

Figure 3. Subthreshold Membrane Potential Regulates PRC changes in Pyramidal Neuron Models.
(**A**) Rate-adaptation of PRCs in the original Traub model. (**B**) Lowered ISI membrane potential at high rates. (**C**) Comparison of ionic currents at low (solid, 7 Hz) and high (dashed, 227 Hz) rates. (**D**) Rate-adaptation of PRCs in the modified Traub model. (**E**) Elevated ISI membrane potential at high rates. (**F**) Comparison of ionic currents at low (solid, 9 Hz) and high (dashed, 49 Hz) rates. In **C** and **F**, current peaks are truncated to show currents during ISIs. In **E**, spike peaks are truncated to show the elevated ISI membrane potential at high rates.

Rate-dependent High-frequency Oscillations

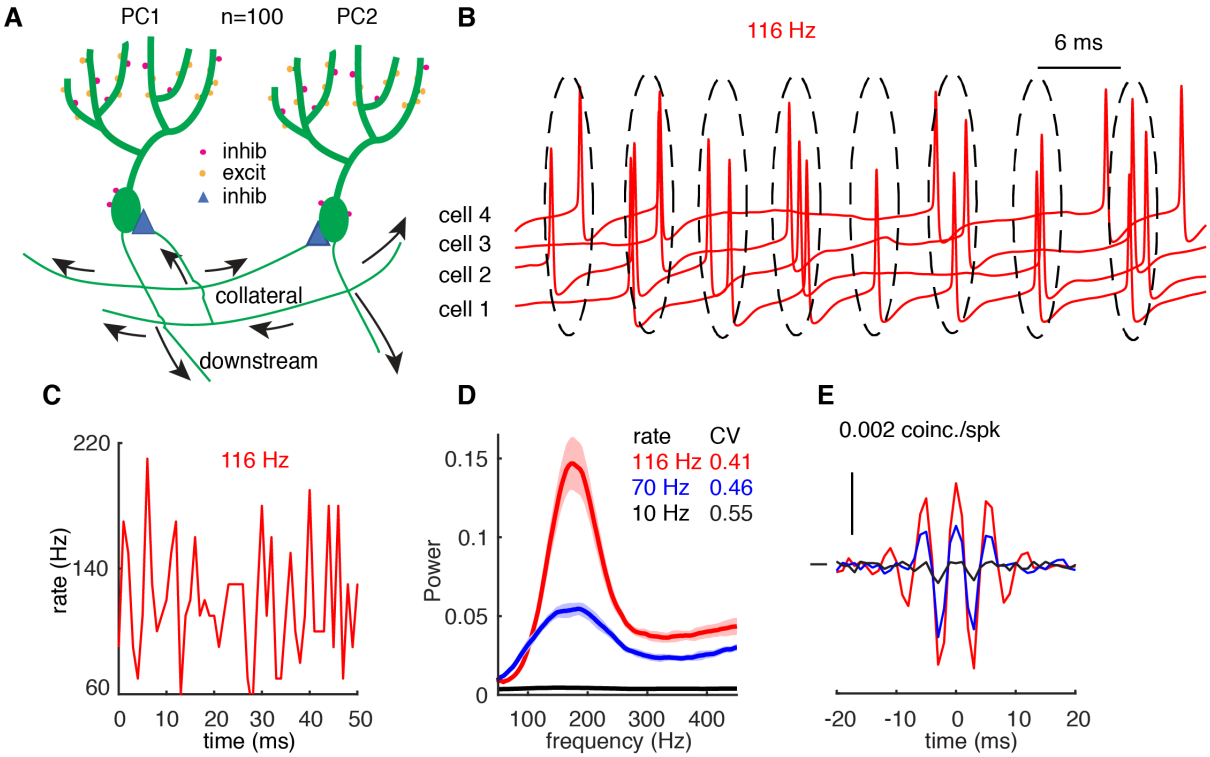

Figure 4. High-frequency Oscillations Show Adaptation with Cellular Spike Rates. (**A**) Schematic representation of the network configuration. (**B**) Example of sampled PC voltage trajectories in the network. (**C**) Example of population rates in the network. (**D**) The power spectrum of population rates of the network at different cellular rates and firing irregularity (CV of ISIs). (**E**) Averaged normalized cross-correlations at different cellular rates.

The potential effect of rate-caused variations of cellular response properties on population synchrony has been largely ignored in previous studies (Bartos et al., 2002; Brunel and Hakim, 1999; de Solages et al., 2008; Heck et al., 2007; Shin and De Schutter, 2006). Here, we examine whether rate correlates with synchrony in the presence of high-frequency oscillations that have been observed in the cerebellar cortex (Cheron et al., 2004; de Solages et al., 2008). We built a biophysically realistic network model composed of 100 PCs with passive dendrites distributed on the parasagittal plane (Witter et al., 2016). Each PC connects to the somas of its 5 nearest neighboring PCs through inhibitory axon collaterals on each side (Bishop and O'Donoghue, 1986; de Solages et al., 2008; Witter et al., 2016). Rates of each PC are independently driven by parallel fiber synapses, stellate cell synapses, and basket cell synapses (Fig. 4A). More details are in **Methods**.

When the average cellular rate is 116 Hz, PCs in the network tend to fire within interspaced clusters with time intervals of ~ 6 ms (Fig. 4B). However, individual PCs do not fire within every cluster. Therefore, spikes in the network show intermittent pairwise synchrony on the population level rather than spike-to-spike synchrony (Fig. 4B). Each peak in Fig. 4C corresponds to a 'cluster'. Based on the power spectrum, the network oscillates at a frequency of ~ 175 Hz (inverse of the cluster interval, ~ 6 ms), independent of cellular rates (116 Hz in red and 70 Hz in blue, Fig. 4D) because oscillation frequency is mainly determined by synaptic properties (Brunel and Hakim, 1999; de Solages et al., 2008). When cellular rates increase from 70 Hz to 116 Hz, the power of high-frequency oscillations significantly increases and the peak

becomes sharper. When individual PCs fire at low rates (10 Hz), the network fails to generate high-frequency oscillations and each PC fires independently, as evidenced by the flat power spectrum (Fig. 4D). High-frequency oscillations and their rate-dependent changes are also reflected in the average normalized cross-correlograms (CCGs) between PC pairs (Fig. 4E). When PCs fire at 70 Hz and 116 Hz, in addition to positive central peaks, two significant side peaks can be observed in the CCGs, suggesting correlated spikes with 0 ms time lag and ~ 6 ms time lag. Amplitudes of the peaks increase with cellular rates and disappear when the rate is low (10 Hz). Notice that the computed CCG shows 'excess' correlation, which is computed by the raw correlation minus the shift predictor (Heck et al., 2007; Smith and Kohn, 2008).

Effect of Cell and Network Properties on Oscillations

In the previous section, the variation of cellular rates was driven by synaptic input to demonstrate the rate-adaptation of high-frequency oscillations. However, it is difficult to differentiate the relative contribution of PRC shapes and firing irregularity (measured by the CV of ISIs) since they covary with rate (Fig. 4D). Therefore, cellular rates were systematically varied by dynamic current injections, which were approximated by the Ornstein–Uhlenbeck (OU) process (Destexhe et al., 2001). This simulation protocol also causes the formation of high-frequency oscillations (Fig. S2). When PCs fire with low to moderate CV of ISIs, they show loose spike-to-spike synchrony at high rates, but not at low rates. With high CV of ISIs, spikes are jittered and spike-to-spike synchrony is disrupted. High-frequency oscillations were never observed under the condition of low cellular rates.

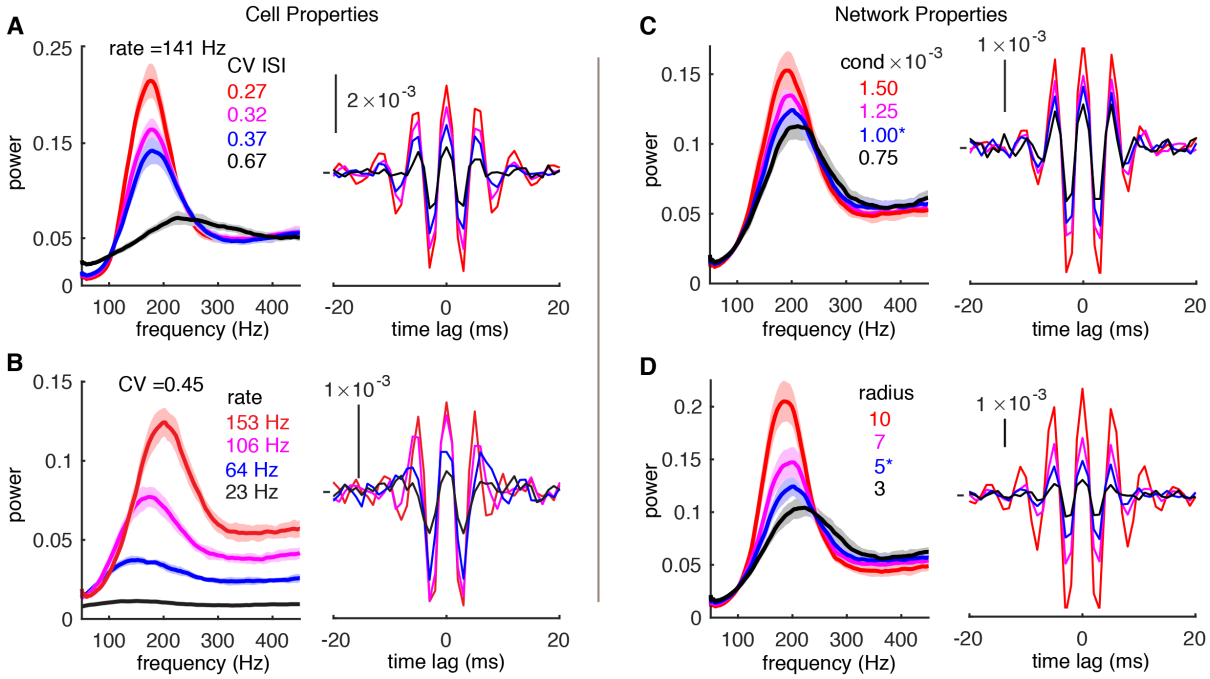

Figure 5. Effect of Cell and Network Properties on High-frequency Oscillations. Both irregular spiking (high CV of ISIs) in **A** or low cellular rates in **B** decorrelate network output in the forms of reduced peaks of power spectrums (left) and CCGs (right). In **A**, the cellular rate is ~ 141 Hz. In **B**, the CV ISI is ~ 0.45. Both small conductance (cond) of inhibitory synapses in **C** and a short connection radius (**D**) decorrelate network output in the forms of reduced peaks of power spectrums (left) and CCGs (right). In A&B, the cond is 1 nS and radius is 5. In **C**&**D**, the cellular rate is ~ 151 Hz and the CV ISI is ~ 0.45.

Both spiking irregularity and rates of PCs covary with cerebellum-associated behaviors (Chen et al., 2016). Our results show that small spiking irregularity supports high-frequency oscillations. However, further increasing spiking irregularity reduces the power of high-

frequency oscillations and makes the power spectrum flatter when rates are the same (141 Hz) (Fig. 5A). In average normalized CCGs, both central and side peaks decrease with increased firing irregularity. Both results suggest reduced correlation when PCs fire very irregularly. Next, we explore how rate-dependent PRCs regulate network output. The power of high-frequency oscillations increases and the power peak becomes sharper with large, broad PRCs at high rates (Fig. 5B). Peaks in the average CCGs also increase, suggesting more correlated spike outputs at high rates. In Fig. S3, we demonstrate that the PRC peak amplitude at high cellular rates controls the oscillation power.

At the circuit level, the strength of inhibitory synapses and connection radius are difficult to determine accurately, but their values are critical for the function of axon collaterals. Within the ranges of experimentally reported synaptic conductance and connection radius (de Solages et al., 2008; Fisyunov et al., 2006; Orduz and Llano, 2007; Watt et al., 2009; Witter et al., 2016), the network generates robust high frequency oscillations (Fig. 5C, D). In addition, we find that increasing the conductance of inhibitory synapses or their connection radius increases the power of high-frequency oscillations and make the power spectrum sharper. The increased oscillation power due to connectivity properties is also captured by the larger peaks in CCGs. Both effects can be explained by larger phase responses due to larger inputs (synaptic connections, Fig. S1C). Together, our simulation data suggest that the correlation between PC spikes is strong under conditions of low to moderate spiking irregularity, high cellular rate, high synaptic conductance, and large connection radius.

Transient Correlations Are Robust to Heterogeneous Spike rates

Although inhibitory connections loosely synchronize spike output and cause oscillations, their functional role will depend on the following answers: When do they occur? How fast can they be achieved? Are they robust to heterogeneous cellular spike rates? We have previously simulated networks with a range of homogeneous stable cellular rates. Here, we first test whether rate-dependent synchrony still holds when population rates change dynamically. Population rates of the network approximate the half-positive cycle of a 1 Hz sine wave (peak ~ 140 Hz) with the duration of each trial being 1 sec (Fig. 6A). We computed shuffle-corrected, normalized joint peristimulus time histograms (JPSTHs) to reflect the dynamic synchrony (Aertsen et al., 1989) (Fig. S4A). The main and the third diagonal of the JPSTH matrix, corresponding to 0 ms time lag correlation and 6 ms time lag correlation respectively, are plotted to show the dynamic synchrony at transiently increased rates (bin size is 2 ms, Fig. 6B). At low basal rates, there are no correlations between spikes. Both correlations start to increase ~ 250 ms after the onset of simulations and decrease again when the cellular rates drop, closely following rate changes. It demonstrates that axon collateral-caused spike correlations can be achieved transiently to transmit a timing signal conjunctive with temporal cellular rate increases.

Although it remains unclear whether the population of PCs converging onto a same cerebellar nuclei neuron are homogeneous or heterogeneous, simultaneous bidirectional PC rate changes have been observed during cerebellum-related behaviors (Chen et al., 2016; Herzfeld et al., 2015). It is very likely that neighboring PCs show heterogeneous spike rate changes, which may reduce spike correlations (Markowitz et al., 2008). Therefore, we distributed 10-30 extra cells with decreased spike rates in the network to test the effect of heterogeneous neighboring rate changes on the transient correlations (The population firing rates of increased-rate cells and decreased-rate cells are shown in Fig. S4B). They were randomly scattered among the cells with increasing rates. Spike correlations still become larger for the subgroup of PCs showing increased cellular rates, despite a slight decrease of the correlation amplitude when more cells decrease their spike rates (Figs. 6C-E). The results suggest that a population of PCs with increased spike rates can form subgroups to propagate

synchrony information even when they are surrounded by non-correlated neighboring PCs with decreased spike rates.

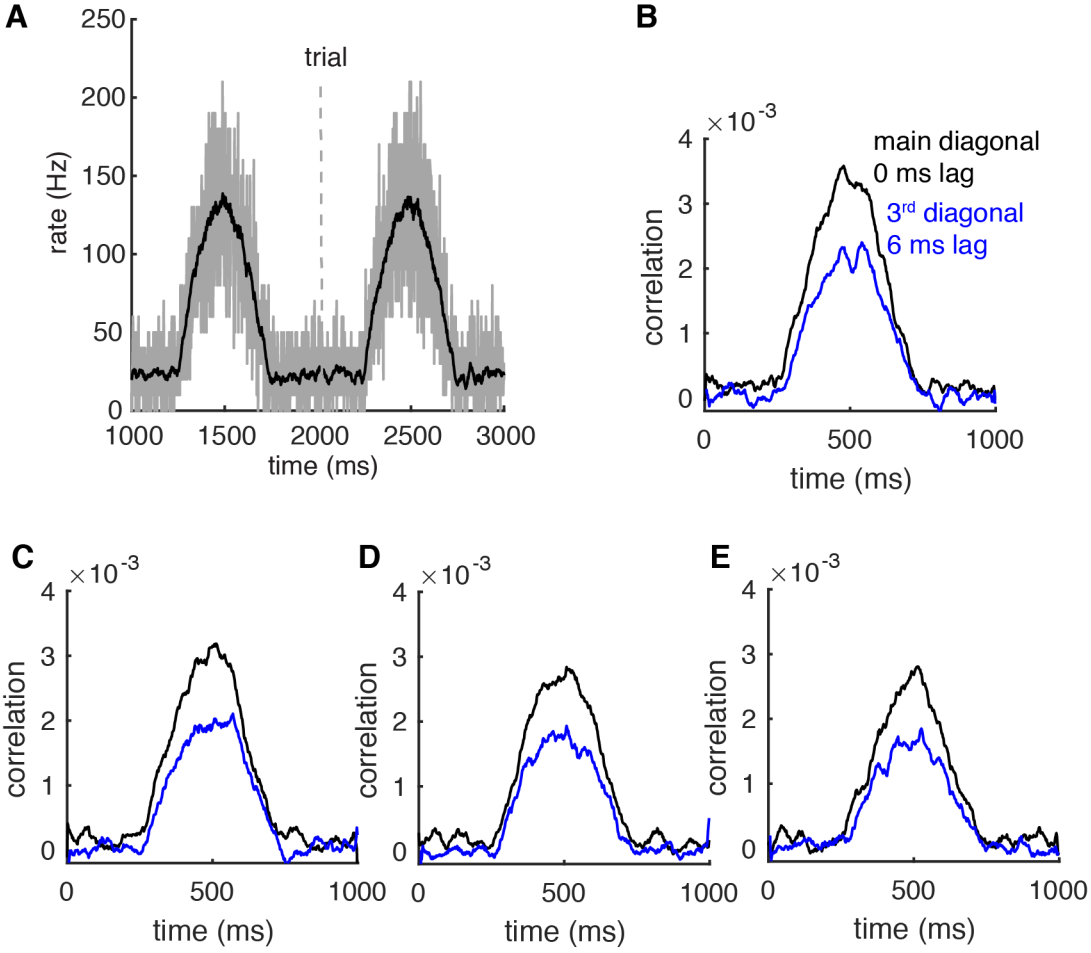

Figure 6. Correlations can be transient and robust to heterogeneous spike rates
(**A)** Population spike rates of PCs. (**B)** The 0 ms- and 6 ms-time lag correlations increase with population rates. (**C-E**) The rate-dependent correlation is robust to heterogeneous cellular rate changes. From **C** to **E**, the number of decreased rate cells increases from 10 to 30.

Discussion

In this work, we dissected biophysical mechanisms shaping PRC profiles and explored their role in synchronizing spikes in cerebellar PCs. We started by reproducing the rate adaptation of PRCs in PCs and then identified rate-modulated interspike potentials as the underlying mechanism. We further demonstrated rate-dependent phase responses can link spike rate with spike timing to regulate neuronal output.

Biophysical Mechanisms Underlying Rate-dependent PRCs

The profiles of neuronal PRCs are rate-dependent (Couto et al., 2015; Ermentrout et al., 2001; Gutkin et al., 2005; Phoka et al., 2010; Tsubo et al., 2007). In cortical neurons, slow voltage-dependent K^+ and Ca^{2+}-activated K^+ currents were proposed to mediate rate adaptation of their PRCs and emergent synchrony between excitatory coupled neurons (Ermentrout et al., 2001; Gutkin et al., 2005). These studies presumed that the decrease of PRC peaks with increasing spike rates would be general for type-I PRCs (always advancing). However, this prediction has not been confirmed in later experiments (Couto et al., 2015; Phoka et al., 2010; Tsubo et al., 2007). In Layer 2/3 pyramidal neurons, PRCs tend to transit from type-I to type-II with increasing rate (advanced or delayed depending on phase) (Tsubo et al., 2007). Even in

neurons preserving type-I PRCs (mainly Layer 5), peaks tend to increase with rate (see Figs. 3E&4 of Tsubo et al. (2007)). Cerebellar PCs exhibit a transition from small, phase-independent responses to large, phase-dependent type-I responses with increasing rate (Couto et al., 2015; Phoka et al., 2010), but the mechanism was unknown (Akemann and Knopfel, 2006; Couto et al., 2015; De Schutter and Bower, 1994; Khaliq et al., 2003; Phoka et al., 2010). This work reproduces and explains the experimentally observed rate adaptation of PRCs. Note that the slight increase of PRCs in the very narrow late phase in our model (low rate, Fig. 1B) may be annihilated by noise in spontaneously firing neurons (Couto et al., 2015; Phoka et al., 2010). Compared with previous work emphasizing the slow deactivation of K^+ currents in cortical neurons (Ermentrout et al., 2001; Gutkin et al., 2005), here we unveil the general role of rate-dependent subthreshold membrane potentials and their corresponding activation of Na^+ currents. In both pyramidal neurons and PCs, spike rates cause significant variation of the subthreshold membrane potential during the ISI (Rancz and Hausser, 2010; Tsubo et al., 2007). In response to a stimulus, both Na^+ and K^+ currents are activated. In PCs, the main K^+ current is high-threshold activated (Martina et al., 2003; Zang et al., 2018); therefore, depolarization-facilitated Na^+ currents dominate, causing larger PRCs at high rates (Fig. 2). However, previous PC models (Akemann and Knopfel, 2006; Couto et al., 2015; De Schutter and Bower, 1994; Khaliq et al., 2003; Phoka et al., 2010) possess low-threshold-activated K^+ currents, which counteract facilitated Na^+ currents, explaining an absence of increased PRCs at high rates. In the Traub model, slow deactivation of K^+ currents and consequent hyperpolarization synergistically reduce the PRC peaks at high rates (Ermentrout et al., 2001; Gutkin et al., 2005). By minimally modifying the Traub model, elevated subthreshold interspike potentials generate larger PRCs peaks at high rates (Fig. 3) as in experiments (Tsubo et al., 2007). To the best of our knowledge, decreased neuronal PRCs at high firing rates haven't been experimentally observed yet.

Spike Synchronization Mechanisms

Whether spike timing carries critical information for cerebellar function is still controversial. For smooth pursuit eye movement in monkeys, the movement was reported to be coded just by PC spike rates (Payne et al., 2019). However, during saccades, the spike timing of some PCs provides a temporally reliable signal for the onset of eye movement (Hong et al., 2016). In mice, well-timed spiking in PCs and cerebellar nuclei neurons is critical in cerebellum-related locomotion and whisking (Brown and Raman, 2018; Sarnaik and Raman, 2018). Therefore, spike timing is important for at least some, if not all, cerebellum-related behaviors. Both synchronized complex spikes (De Gruijl et al., 2014; Tang et al., 2019) and simple spikes (de Solages et al., 2008; Heck et al., 2007; Shin and De Schutter, 2006) have been observed *in vivo*. Among all observations, the high-frequency oscillations (Cheron et al., 2004; de Solages et al., 2008; Groth and Sahin, 2015) do not rely on synchronized afferent input and were proposed to be caused by recurrent inhibitory axon collaterals (de Solages et al., 2008). Recent work has confirmed the presence of recurrent axon collaterals in adult mice by direct imaging and reconstruction (Witter et al., 2016), while they were previously thought to exist in young mice only (Watt et al., 2009). For high-frequency oscillations, rate-dependent phase responses increase the oscillation level at high rates, with no need to increase afferent input correlation. Note that rate-related synchrony can also be achieved via common synaptic inputs (Heck et al., 2007), gap junctions (Middleton et al., 2008), and ephaptic coupling (Han et al., 2018), when the inputs or connections are weak. To achieve synchrony, neuronal PRCs are required to be none-zero, regardless of the driving mechanism. For larger PRC values, advanced spikes, or those delayed by inhibition, will be more clustered relative to the stimuli (Ermentrout et al., 2008). Since synchronization mechanisms are not mutually exclusive, they may work synergistically to achieve the required synchrony level. However, rate-dependent PRCs will

not help synchronize complex spikes triggered by common or correlated climbing fiber inputs (De Gruijl et al., 2014; Tang et al., 2019), because the inputs are powerful enough to evoke spikes immediately.

The Evidence Supporting Rate-dependent Correlations

There is no direct experimental data supporting rate-dependent synchrony in the cerebellum. However, careful analysis of previous experimental data in the cerebellum provides some evidence to support our findings. In the work of de Solages et al. (2008), units with lower average rates (<10 Hz) did not exhibit significant correlations between neighboring PCs, for unknown reasons. This can be explained by the small flat PRCs at low rates. Under extreme conditions, when the PRC is constantly 0 (equivalent to disconnection), no correlations can be achieved (Figs. 4-6). Additionally, the oscillation power increased by the application of WIN 55,212-2, which was intended to suppress background excitatory and inhibitory synapses (de Solages et al., 2008). The increased power could be due to more regular spiking after inhibiting the activity of background synapses (Fig. 5A). However, it could also be caused by increased spike rates (Fig. 5B), because this agent also blocks P/Q type Ca^{2+} channels and consequently P/Q type Ca^{2+}-activated K^{+} currents, to increase spike rates (Fisyunov et al., 2006). Similarly, enhanced oscillations have also been observed in calcium-binding protein gene KO mice, which accompany significantly higher simple spike rates (Cheron et al., 2004).

Spatio-temporal Correlated Spiking

We built a link between oscillation level and firing irregularity (Fig. 5A). Given that increased firing irregularity is usually linked to cerebellar dysfunction (Peter et al., 2016; Walter et al., 2006), our results imply that irregularity-disrupted temporal population firing patterns can be the ultimate reason. Although temporal synchrony may carry important timing information for the onset of some movements (Brown and Raman, 2018; Hong et al., 2016; Sarnaik and Raman, 2018), optimal cerebellar function seems to occur between excessive asynchrony and synchrony (Shakkottai, 2014). It has been shown that synchronized simple spikes are time-locked to reaching-grasping movements in rats (Heck et al., 2007). Before and after such movements, synchronized simple spikes were not observed. High-frequency oscillations time-locked to lever-pressing in rats have been reported (Groth and Sahin, 2015). Additionally, in humans high-gamma oscillations in the cerebellar cortex significantly increase during a reaching task (Carver et al., 2019). Nonetheless, global and rhythmic increased synchrony (Cheron et al., 2004) may abrogate normal separation of timing signals to different muscle groups (for example agonist and antagonist muscles), causing impaired motor coordination, such as dystonia (Shakkottai, 2014). In our model, PRCs are quantitatively close to experimental data (Fig. 1). When cell and network parameters fall within physiological ranges (Figs. 5,6), the network shows very weak oscillations at low basal cellular rates, but the PC ensemble can dynamically increase the correlation level within a subgroup of PCs with increased rates (Person and Raman, 2011) (Fig. 6). Local gamma oscillations have been shown to selectively route input information in a cortical circuit model (Palmigiano et al., 2017). Similarly, in the cerebellum, temporal information can be transiently separated and directed to different subgroups of PCs to efficiently coordinate muscle movements. Thus, the spatial range of axon collaterals (~ 210 µm, each connecting 7 to 10 neighboring PCs (Bishop and O'Donoghue, 1986; Watt et al., 2009; Witter et al., 2016)), the strength of their synapses (on the order of 1 ns (de Solages et al., 2008; Orduz and Llano, 2007; Witter et al., 2016)), and rate-dependent PRCs (Couto et al., 2015; Phoka et al., 2010) may well be configured to support spatio-temporal synchrony at high rates. Furthermore, when PCs fire at high rates, the strong facilitation of inhibitory axon collateral synapses may be a complementary mechanism to strengthen this dynamic synchrony (Orduz and Llano, 2007).

Possible Rate-dependent Oscillations in Hippocampus

The high-frequency oscillations in the cerebellum are reminiscent of hippocampal ripple oscillations involved in memory consolidation. Ripple oscillations are thought to originate from parvalbumin-expressing GABAergic neuron networks (Bartos et al., 2002). PCs and hippocampal GABAergic neurons both are fast-spiking inhibitory neurons. They have similar f-I curve slopes and their principal repolarization currents both are Kv3 currents (Hu et al., 2018). Thus, it will be interesting to explore whether PRCs of GABAergic neurons and the power of ripple oscillations exhibit similar rate adaptations.

Conclusion

We have identified the subthreshold membrane potential as a general mechanism shaping neuronal PRC profiles. It will help experimentalists and theorists to understand and reproduce measured PRCs, and further explore their function in encoding temporal information in different circuits. Rate-dependent phase responses couple spike rate with spike timing, which may be a significant neuronal property to spatio-temporally regulate their outputs.

Acknowledgement

YLZ and EDS would like to thank the helpful suggestions from Drs. Eve Marder, Tomoki Fukai, Sungho Hong and Sergio Verduzco to improve the manuscript and the language editing by Steven Douglas Aird.

Methods

The detailed PC model and the interconnected network model were implemented in NEURON 7.5 (Carnevale and Hines, 2006). The Traub model was implemented in MATLAB. The code used in this work will be available from ModelDB.

PRC computations

Our recently developed compartment-based PC model was used (Zang et al., 2018). To compute the PRCs in Fig. 1, brief current pulses with a duration of 0.5 ms and an amplitude of 50 pA were administered at the soma at different phases of interspike intervals. The resulting perturbed periods were then used to calculate phase advances by the formulation $PRC = (< ISI > - ISI_{perturb}) / < ISI >$. Different cellular rates were achieved by somatic holding currents (Couto et al., 2015; Phoka et al., 2010). To compute PRCs in response to negative stimuli, the amplitudes of the pulses were changed to - 50 pA. To compute PRCs of our PC model with passive dendrites, only H current and leak current were distributed on the dendrites with the same parameters as in the active model (Zang et al., 2018). The Traub model (Traub et al., 1999) was implemented according to the work of Ermentrout et al (Ermentrout et al., 2001; Gutkin et al., 2005). In the modified version of this model, the conductance of the kdr current was reduced from 80 to 40. Activation and deactivation rates of this current were shifted to the right by 30 mV, $\alpha_n(v) = 0.032*(v+22)/(1-\exp(-(v+22)/5))$; $\beta_n(v) = 0.5*\exp(-(v+27)/40)$; the conductance of AHP current was increased from 0 to 0.1.

Network simulations

We implemented our recurrent inhibitory PC layer network using the Watts-Strogatz model (Watts and Strogatz, 1998) to avoid boundary effects. To reduce simulation time, we used the PC model with passive dendrites, which exhibits similar rate-dependent PRCs as the PC model with active dendrites (Fig. S1B). In the baseline version of the network, 100 PCs were

distributed on the parasagittal plane (Witter et al., 2016), corresponding to 2 mm of folium with a distance of 20 μm between neighboring PC soma centers. 100 PCs are within the estimated range of PCs converging to a same cerebellar nuclei neuron (Person and Raman, 2011). Each PC was connected to its nearest 2*radius neighboring PC somas and connections had 0 rewiring probability. The PCs were interconnected, according to anatomical data showing collaterals present toward both the apex and the base of the lobule with only slight directional biases (Witter et al., 2016). The baseline value of radius was 5 within the range of experimental estimates (de Solages et al., 2008; Watt et al., 2009; Witter et al., 2016). The inhibitory postsynaptic current (IPSC) was implemented using the NEURON built-in point process, Exp2Syn. G = weight * (exp(-t/τ_2) - exp(-t/τ_1)), with τ_1 = 0.5 ms (rise time) and τ_2 = 3 ms (decay time). The reversal potential of the IPSC was set at -85 mV (Watt et al., 2009). The conductance was 1 nS (de Solages et al., 2008; Orduz and Llano, 2007; Witter et al., 2016). The delay between onset of an IPSC and its presynaptic spike timing was 1.5 ms (de Solages et al., 2008; Orduz and Llano, 2007; Witter et al., 2016). To test the effect of rate-dependent PRCs on high-frequency oscillations, we varied the cellular rates in two paradigms. In the first (Fig. 4), each PC is contacted by 4,000 excitatory parallel fiber synapses (PF, on spiny dendrites), 18 inhibitory stellate cells (STs, on spiny dendrites) and 4 inhibitory basket cells (BSs, on the soma). Activation of excitatory and inhibitory synapses in each PC was approximated as an independent Poisson process with different rates. We simulated 3 conditions: PC rate = 10 Hz when PF rate = 0.27 Hz, ST rate = 14.4 Hz, BS rate = 14.4 Hz; PC rate = 70 Hz when PF rate = 2.16 Hz, ST rate = 28.8 Hz, BS rate = 28.8 Hz; PC rate = 116 Hz when PF rate = 3.24 Hz, ST rate = 28.8 Hz, BS rate = 28.8 Hz. To more systematically explore different factors regulating network outputs, after Fig.4, we used a second paradigm. Cellular rates of each PC were manipulated by injecting stochastic currents on the soma. The stochastic current was approximated by the commonly used Ornstein-Uhlenbeck random process (Destexhe et al., 2001), $\tau\frac{dI}{dt} = -I + \sigma\sqrt{\tau}\eta_i(t)$. σ represents the amplitude of the fluctuation; η_i represents uncorrelated white noise with unit variance; $\tau = 5$ ms. In this paradigm, we systematically varied the rates and firing irregularities of PCs (CV of ISIs) to explore their importance for network output. Phase response is a result of input current and response gain of the cell. No existing data support decreased PRC at high cellular rates. In our model, in a physiological range, it is not available either. We therefore reduce the phase response by halving the input current (synaptic conductance) to achieve a smaller response at high firing rates (Fig. S3). We also explored the effect of connection radius with the values of 3, 5, 7 and10 in Fig. 5D. The conductance of inhibitory synapses was tested with the values of 0.75, 1.0, 1.25 and 1.5 ns in Fig. 5C. To test the spatio-temporally increased correlation, we randomly distributed extra 10 - 30 PCs with decreased cellular rates into the original network (Fig. 6), including 100 increased-rate cells. Their mean population firing rates are shown in Fig. S4B.

Data analysis

The power spectrum of the spike trains of the network was estimated by Welch's method, which calculates the average of the spectra of windowed segments (window size 128 points). In each trial under each specific stimulus condition, the length of the signal was 2 sec, with a time resolution of 1 msec. The final result was the average of 14 trials.

To compute the cross-correlogram (CCG) under each specific stimulus condition, we first computed pairwise correlations between the spike trains of two neurons and then corrected them by shift predictors, which removed the 'chance correlations' due to rate changes. Then correlations were divided by the triangular function $\Theta(\tau) = T - |\tau|$ and $\sqrt{\lambda_i\lambda_j}$. T was the duration of each trial and τ was the time lag. $\Theta(\tau)$ corrects for the degree of overlap between two spike trains for each time lag τ. λ_i was the mean firing rate of neuron *i* (Kohn and Smith,

2005). Finally, the CCGs between all pairs in the network were averaged to reflect the population level spike correlations. Thus, similar with previous work (Heck et al., 2007), the computed CCGs reflect the 'excess' correlation caused by axon collaterals in our work. To measure the dynamic correlation over the time course of the stimulus, we computed JPSTHs. Here we used a 2-ms time bins due to the narrow central peak and side peaks. Larger time bins annihilated the positive peaks due to the significant negative correlations in paired spikes. Therefore, we simulated 1992 trials to compute the raw JPSTH between PC pairs. Similar with CCGs, the raw JPSTH was corrected by subtracting the shift predictor (cross-product matrix of individual peri-event time histograms) to remove the coincident spikes due to rate changes and co-stimulus. The corrected JPSTH was then normalized by the squared root of product of each neuron's PSTH standard deviations (Aertsen et al., 1989). The corrected matrix values become correlation coefficients, with values between -1 and +1. Finally, all pair-wise JPSTHs were averaged to reflect the population level dynamic correlations.

References

Aertsen, A.M., Gerstein, G.L., Habib, M.K., and Palm, G. (1989). Dynamics of neuronal firing correlation: modulation of "effective connectivity". J Neurophysiol *61*, 900-917.

Akemann, W., and Knopfel, T. (2006). Interaction of Kv3 potassium channels and resurgent sodium current influences the rate of spontaneous firing of Purkinje neurons. J Neurosci *26*, 4602-4612.

Bartos, M., Vida, I., Frotscher, M., Meyer, A., Monyer, H., Geiger, J.R., and Jonas, P. (2002). Fast synaptic inhibition promotes synchronized gamma oscillations in hippocampal interneuron networks. Proc Natl Acad Sci U S A *99*, 13222-13227.

Bishop, G.A., and O'Donoghue, D.L. (1986). Heterogeneity in the pattern of distribution of the axonal collaterals of Purkinje cells in zone b of the cat's vermis: an intracellular HRP study. J Comp Neurol *253*, 483-499.

Brown, S.T., and Raman, I.M. (2018). Sensorimotor Integration and Amplification of Reflexive Whisking by Well-Timed Spiking in the Cerebellar Corticonuclear Circuit. Neuron *99*, 564-575 e562.

Brunel, N., and Hakim, V. (1999). Fast global oscillations in networks of integrate-and-fire neurons with low firing rates. Neural Comput *11*, 1621-1671.

Carnevale, N.T., and Hines, M.L. (2006). The NEURON book (Cambridge, UK ; New York: Cambridge University Press).

Carver, F.W., Sepe-Forrest, L., Quentin, R., Holroyd, T., Coppola, R., and Nugent, A.C. (2019). Cerebellar high gamma activation during performance of a reaching task in MEG. In Society for Neuroscience (Chicago, IL: online).

Chen, S., Augustine, G.J., and Chadderton, P. (2016). The cerebellum linearly encodes whisker position during voluntary movement. Elife *5*, e10509.

Cheron, G., Gall, D., Servais, L., Dan, B., Maex, R., and Schiffmann, S.N. (2004). Inactivation of calcium-binding protein genes induces 160 Hz oscillations in the cerebellar cortex of alert mice. J Neurosci *24*, 434-441.

Couto, J., Linaro, D., De Schutter, E., and Giugliano, M. (2015). On the firing rate dependency of the phase response curve of rat Purkinje neurons in vitro. PLoS Comput Biol *11*, e1004112.

De Gruijl, J.R., Hoogland, T.M., and De Zeeuw, C.I. (2014). Behavioral correlates of complex spike synchrony in cerebellar microzones. J Neurosci *34*, 8937-8947.

De Schutter, E., and Bower, J.M. (1994). An active membrane model of the cerebellar Purkinje cell. I. Simulation of current clamps in slice. J Neurophysiol *71*, 375-400.

de Solages, C., Szapiro, G., Brunel, N., Hakim, V., Isope, P., Buisseret, P., Rousseau, C., Barbour, B., and Lena, C. (2008). High-frequency organization and synchrony of activity in the purkinje cell layer of the cerebellum. Neuron *58*, 775-788.

Destexhe, A., Rudolph, M., Fellous, J.M., and Sejnowski, T.J. (2001). Fluctuating synaptic conductances recreate in vivo-like activity in neocortical neurons. Neuroscience *107*, 13-24.

Ermentrout, B., Pascal, M., and Gutkin, B. (2001). The effects of spike frequency adaptation and negative feedback on the synchronization of neural oscillators. Neural Comput *13*, 1285-1310.

Ermentrout, G.B., Galan, R.F., and Urban, N.N. (2008). Reliability, synchrony and noise. Trends Neurosci *31*, 428-434.

Fisyunov, A., Tsintsadze, V., Min, R., Burnashev, N., and Lozovaya, N. (2006). Cannabinoids modulate the P-type high-voltage-activated calcium currents in purkinje neurons. J Neurophysiol *96*, 1267-1277.

Groth, J.D., and Sahin, M. (2015). High frequency synchrony in the cerebellar cortex during goal directed movements. Front Syst Neurosci *9*, 98.

Gutkin, B.S., Ermentrout, G.B., and Reyes, A.D. (2005). Phase-response curves give the responses of neurons to transient inputs. J Neurophysiol *94*, 1623-1635.

Han, K.S., Guo, C., Chen, C.H., Witter, L., Osorno, T., and Regehr, W.G. (2018). Ephaptic Coupling Promotes Synchronous Firing of Cerebellar Purkinje Cells. Neuron *100*, 564-578 e563.

Heck, D.H., Thach, W.T., and Keating, J.G. (2007). On-beam synchrony in the cerebellum as the mechanism for the timing and coordination of movement. P Natl Acad Sci USA *104*, 7658-7663.

Herzfeld, D.J., Kojima, Y., Soetedjo, R., and Shadmehr, R. (2015). Encoding of action by the Purkinje cells of the cerebellum. Nature *526*, 439-442.

Hong, S., Negrello, M., Junker, M., Smilgin, A., Thier, P., and De Schutter, E. (2016). Multiplexed coding by cerebellar Purkinje neurons. Elife *5*.

Hu, H., Roth, F.C., Vandael, D., and Jonas, P. (2018). Complementary Tuning of Na(+) and K(+) Channel Gating Underlies Fast and Energy-Efficient Action Potentials in GABAergic Interneuron Axons. Neuron *98*, 156-165 e156.

Khaliq, Z.M., Gouwens, N.W., and Raman, I.M. (2003). The contribution of resurgent sodium current to high-frequency firing in Purkinje neurons: an experimental and modeling study. J Neurosci *23*, 4899-4912.

Kohn, A., and Smith, M.A. (2005). Stimulus dependence of neuronal correlation in primary visual cortex of the macaque. J Neurosci *25*, 3661-3673.

Markowitz, D.A., Collman, F., Brody, C.D., Hopfield, J.J., and Tank, D.W. (2008). Rate-specific synchrony: Using noisy oscillations to detect equally active neurons. P Natl Acad Sci USA *105*, 8422-8427.

Martina, M., Yao, G.L., and Bean, B.P. (2003). Properties and functional role of voltage-dependent potassium channels in dendrites of rat cerebellar Purkinje neurons. J Neurosci *23*, 5698-5707.

Middleton, S.J., Racca, C., Cunningham, M.O., Traub, R.D., Monyer, H., Knopfel, T., Schofield, I.S., Jenkins, A., and Whittington, M.A. (2008). High-frequency network oscillations in cerebellar cortex. Neuron *58*, 763-774.

578 Orduz, D., and Llano, I. (2007). Recurrent axon collaterals underlie facilitating synapses
579 between cerebellar Purkinje cells. Proc Natl Acad Sci U S A *104*, 17831-17836.
580 Palmigiano, A., Geisel, T., Wolf, F., and Battaglia, D. (2017). Flexible information routing by
581 transient synchrony. Nat Neurosci *20*, 1014-1022.
582 Payne, H.L., French, R.L., Guo, C.C., Nguyen-Vu, T.B., Manninen, T., and Raymond, J.L.
583 (2019). Cerebellar Purkinje cells control eye movements with a rapid rate code that is
584 invariant to spike irregularity. Elife *8*.
585 Person, A.L., and Raman, I.M. (2011). Purkinje neuron synchrony elicits time-locked spiking
586 in the cerebellar nuclei. Nature *481*, 502-505.
587 Peter, S., Ten Brinke, M.M., Stedehouder, J., Reinelt, C.M., Wu, B., Zhou, H., Zhou, K., Boele,
588 H.J., Kushner, S.A., Lee, M.G*., et al.* (2016). Dysfunctional cerebellar Purkinje cells contribute
589 to autism-like behaviour in Shank2-deficient mice. Nat Commun *7*, 12627.
590 Phoka, E., Cuntz, H., Roth, A., and Hausser, M. (2010). A new approach for determining
591 phase response curves reveals that Purkinje cells can act as perfect integrators. PLoS
592 Comput Biol *6*, e1000768.
593 Rancz, E.A., and Hausser, M. (2010). Dendritic spikes mediate negative synaptic gain control
594 in cerebellar Purkinje cells. Proc Natl Acad Sci U S A *107*, 22284-22289.
595 Sarnaik, R., and Raman, I.M. (2018). Control of voluntary and optogenetically perturbed
596 locomotion by spike rate and timing of neurons of the mouse cerebellar nuclei. Elife *7*.
597 Shakkottai, V.G. (2014). Physiologic changes associated with cerebellar dystonia. Cerebellum
598 *13*, 637-644.
599 Shin, S.L., and De Schutter, E. (2006). Dynamic synchronization of Purkinje cell simple spikes.
600 J Neurophysiol *96*, 3485-3491.
601 Smeal, R.M., Ermentrout, G.B., and White, J.A. (2010). Phase-response curves and
602 synchronized neural networks. Philos Trans R Soc Lond B Biol Sci *365*, 2407-2422.
603 Smith, M.A., and Kohn, A. (2008). Spatial and temporal scales of neuronal correlation in
604 primary visual cortex. J Neurosci *28*, 12591-12603.
605 Tang, T., Blenkinsop, T.A., and Lang, E.J. (2019). Complex spike synchrony dependent
606 modulation of rat deep cerebellar nuclear activity. Elife *8*.
607 Traub, R.D., Jefferys, J.G.R., and Whittington, M.A. (1999). Fast oscillations in cortical circuits
608 (Cambridge, Mass.: MIT Press).
609 Tsubo, Y., Takada, M., Reyes, A.D., and Fukai, T. (2007). Layer and frequency dependencies
610 of phase response properties of pyramidal neurons in rat motor cortex. Eur J Neurosci *25*,
611 3429-3441.
612 Walter, J.T., Alvina, K., Womack, M.D., Chevez, C., and Khodakhah, K. (2006). Decreases in
613 the precision of Purkinje cell pacemaking cause cerebellar dysfunction and ataxia. Nat
614 Neurosci *9*, 389-397.
615 Watt, A.J., Cuntz, H., Mori, M., Nusser, Z., Sjostrom, P.J., and Hausser, M. (2009). Traveling
616 waves in developing cerebellar cortex mediated by asymmetrical Purkinje cell connectivity.
617 Nat Neurosci *12*, 463-473.
618 Watts, D.J., and Strogatz, S.H. (1998). Collective dynamics of 'small-world' networks. Nature
619 *393*, 440-442.
620 Witter, L., Rudolph, S., Pressler, R.T., Lahlaf, S.I., and Regehr, W.G. (2016). Purkinje Cell
621 Collaterals Enable Output Signals from the Cerebellar Cortex to Feed Back to Purkinje Cells
622 and Interneurons. Neuron *91*, 312-319.
623 Zang, Y., Dieudonne, S., and De Schutter, E. (2018). Voltage- and Branch-Specific Climbing
624 Fiber Responses in Purkinje Cells. Cell Rep *24*, 1536-1549.

625
626

Supplementary figures

Figure S1. Rate-dependent PRCs.

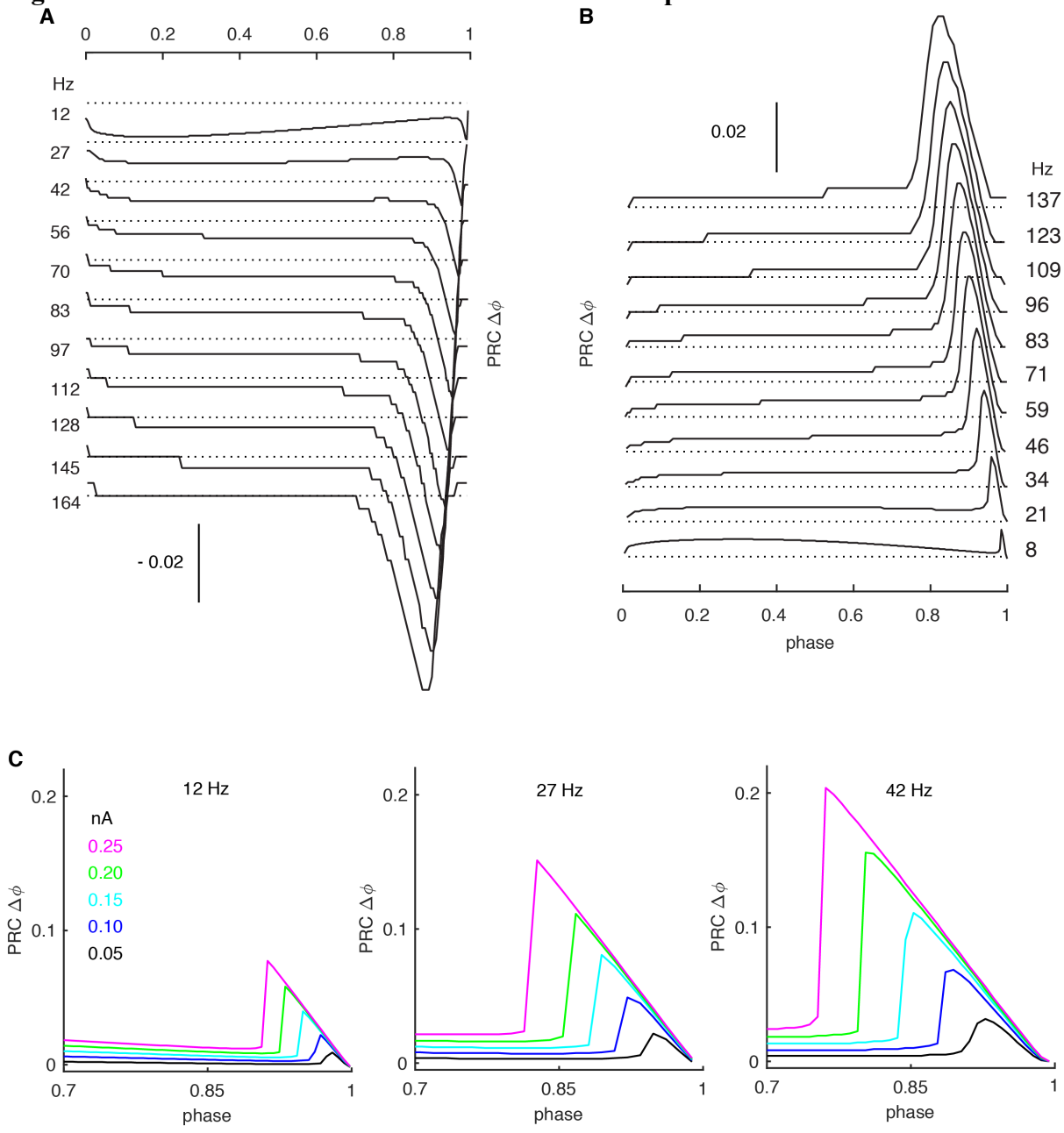

(**A**) Negative stimulus-triggered responses (phase delay) parallel positive stimuli (see Fig .1). Onset-phases of phase-dependent responses shift left at high rates with gradually larger amplitudes. (**B**) The PC model with passive dendrites shows similar rate adaptation as in PC models with active dendrites (Fig. 1). (**C**) Larger stimulus amplitudes increase the peak of the phase-dependent PRCs and shift their onset phases to the left. Simulation results at rates of 12-, 27- and 42-Hz are shown with increased stimulus amplitudes from 0.05 nA to 0.25 nA.

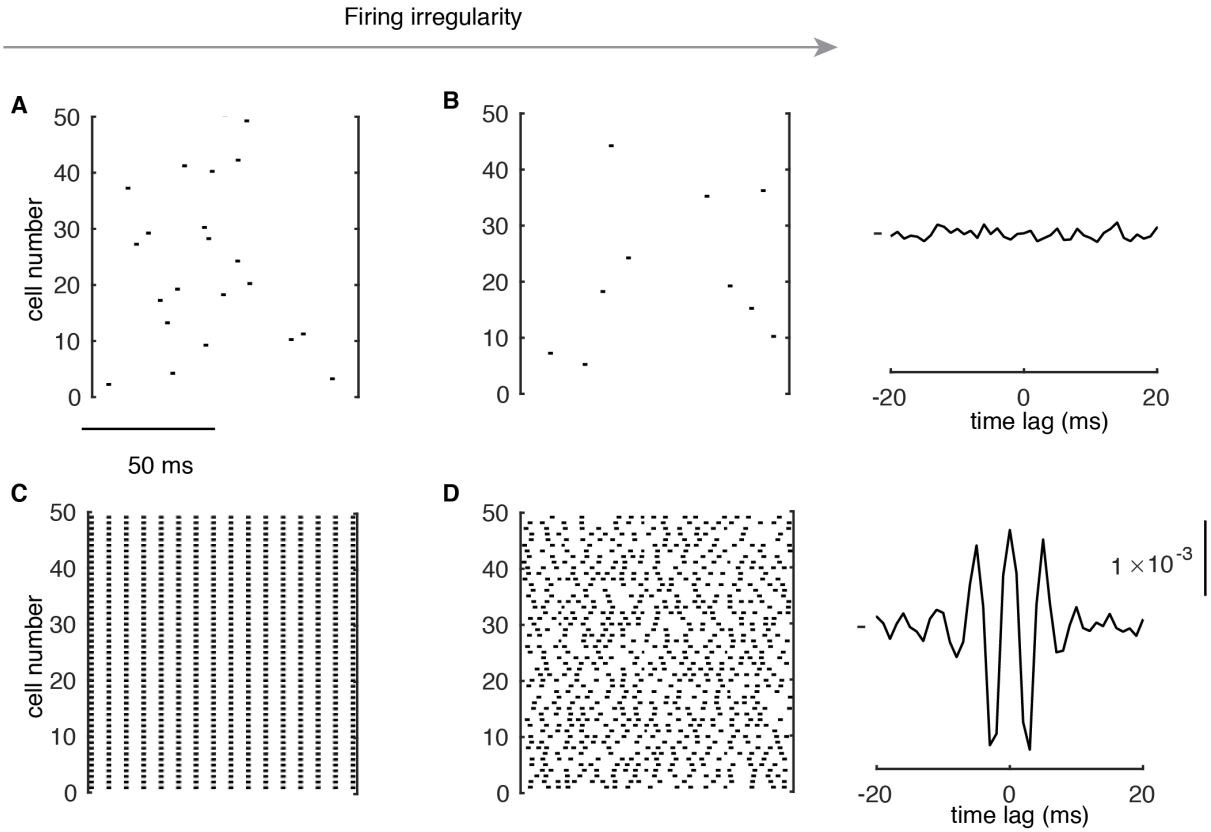

Figure S2. Formation of High-frequency Oscillations at High Rates.
(**A&B**) Raster plots of random PC spikes when they fire regularly (CV ISI ~ 0.07) and irregularly (CV ISI ~ 0.4) at low rates (here, ~ 2 Hz in the network, but 12 Hz in isolated cells). In the right plot of **B**, average CCG is shown. (**C**) PCs show spike-to-spike synchrony when they fire regularly (CV ISI ~ 0.02) at high rates (154 Hz). (**D**) PC spikes show high-frequency oscillations when they fire irregularly (CV ISI ~ 0.44) at high rates (153 Hz). The right plot of **D** shows the average CCG with a significant central peak and side peaks.

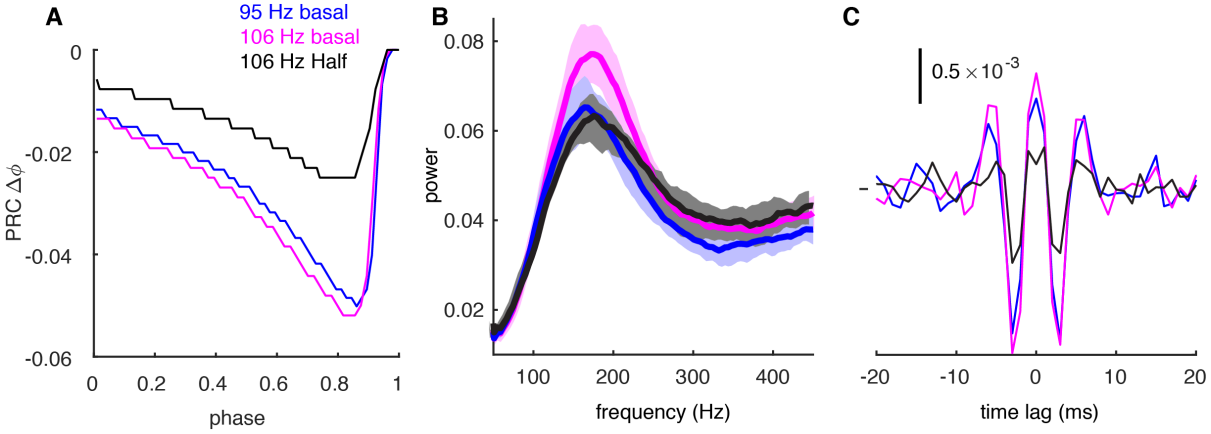

Figure S3. Decreased PRC at High Firing Rates Can Weaken Oscillations.
A. PRCs for negative stimulus (Fig. 1A) when PCs fire at 95 Hz (blue) and 106 Hz (purple) with basal values of synaptic conductance. Reduced PRC at 106 Hz was achieved by 50% of basal synaptic conductance (black). **B**. The power spectrum of spike trains with the cellular rate of 95 Hz (blue, basal conductance), 106 Hz (purple, basal conductance) and 113 Hz (black,

50% of basal conductance, firing rate increased to 113 Hz due to the reduced inhibition, with other conditions the same as 106 Hz with basal conductance). In all cases, the CV of ISI is 0.45. The power spectrum at high firing rates gets flatter with lower amplitude when the PRC amplitude is reduced (black trace). **C**. The CCGs of spike trains with the same condition as in B. Central and side peaks reduce at high firing rates when phase response is smaller.

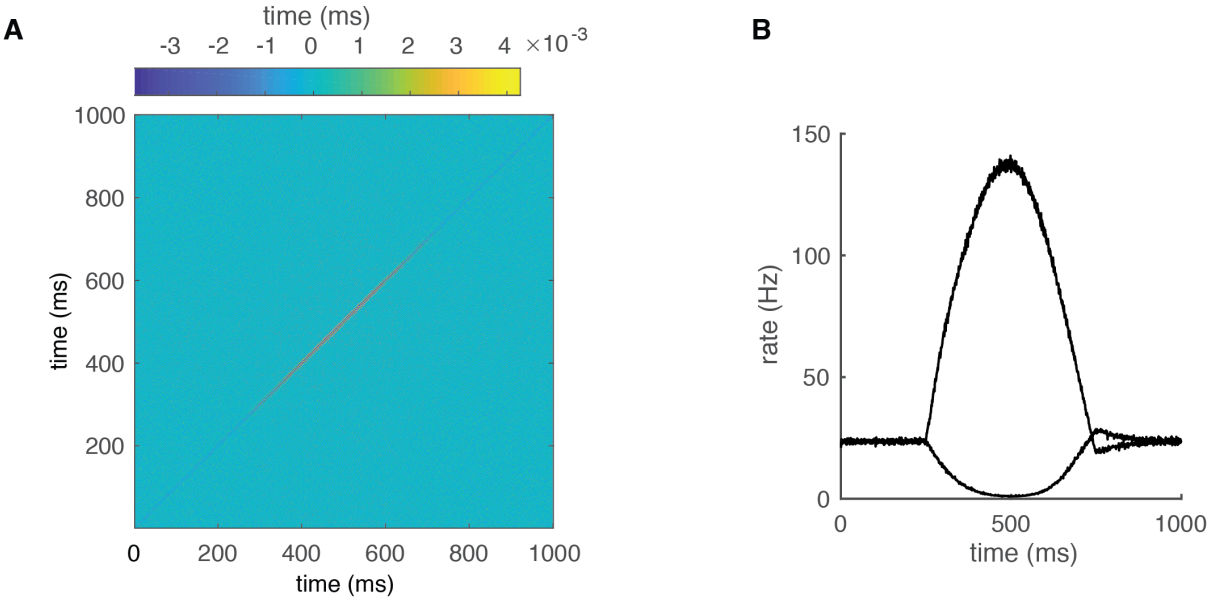

Figure S4. Dynamic Correlations of the PC Network Outputs (Correspond to Fig. 6). **A**. the JPSTH used to produce Fig. 6B. **B**, Population Firing rates of Increased-rate Cells and Decreased-rate Cells for Fig. 6C-E.